



1 **Organic Pollutant Oxidation on Manganese Oxides in Soils - The**  
2 **Role of Calcite Indicated by Geoelectrical and Chemical Analyses**

3 Sonya S. Altzitser<sup>1</sup>, Yael G. Mishael<sup>1</sup>, Nimrod Schwartz<sup>1</sup>

4 <sup>1</sup> Department of Soil and Water Sciences, The Robert H. Smith Faculty of Agriculture, Food and Environment, The  
5 Hebrew University of Jerusalem, Rehovot, 7610001, Israel

6 *Correspondence to:* Nimrod Schwartz ([Nimrod.schwartz@mail.huji.ac.il](mailto:Nimrod.schwartz@mail.huji.ac.il))



7 **Abstract.** Understanding phenolic pollutants interaction with soil colloids has been a focus of extensive research,  
8 primarily under controlled conditions. This study addresses the need to explore these processes in a more natural,  
9 complex soil environment. We aim to enlighten the underlying mechanisms of hydroquinone (a representative  
10 phenolic pollutant) oxidation in ambient,  $\text{MnO}_2$ -rich sandy soil within soil columns designed for breakthrough  
11 experiments. Our innovative approach combines noninvasive electrical measurements, crystallographic and  
12 microscopic analyses, and chemical profiling to comprehensively understand soil-pollutant interactions. Our study  
13 reveals that hydroquinone oxidation by  $\text{MnO}_2$  initiates a cascade of reactions, altering local pH, calcite dissolution,  
14 and precipitating amorphous Mn-oxides, showcasing a complex interplay of chemical processes. Our analysis,  
15 combining insights from chemistry and electrical measurements, reveals the oxidation process led to a constant  
16 decrease in polarizing surfaces, as indicated by quadrature conductivity monitoring. Furthermore, dynamic shifts in  
17 the soil solution chemistry (changes in the calcium and manganese concentrations, pH, and EC) correlated with the  
18 non-monotonous behavior of the in-phase conductivity. Our findings conclusively demonstrate that the noninvasive  
19 electrical method allows real-time monitoring of calcite dissolution, serving as a direct cursor to the oxidation process  
20 of hydroquinone, enabling the observation of soil surface processes, and chemical interactions.



## 21 1. Introduction

22 Phenolic pollutants may originate from various sources, including agricultural, industrial, municipal, and medical  
23 wastes (Davi and Gnudi, 1999; Farhan Hanafi and Sapawe, 2020). Due to their chemical characteristics, phenolic  
24 pollutants tend to persist in soil and water at relatively low concentrations for an extended period, posing a significant  
25 environmental threat. The chemical fate of these pollutants in soil has been extensively studied, with particular  
26 attention given to processes such as adsorption-desorption and oxidation (Ahmed et al., 2015; Delgado-Moreno et al.,  
27 2021; Kang and Choi, 2008; Lambert, 2018; Loffredo and Senesi, 2006; Sun et al., 2022). Regarding oxidation,  
28 various oxides, both natural and engineered, have been investigated for their potential to remove phenolic pollutants  
29 (Gusain et al., 2019; Remucal and Ginder-Vogel, 2014). Among these, birnessite ( $\text{MnO}_2$ ), a manganese oxide naturally  
30 found in soils, is known for its effectiveness in oxidizing various phenolic compounds (Murray, 1974; Remucal and  
31 Ginder-Vogel, 2014).

32 While manganese oxides' ability to oxidize phenols has been explored widely, most of these studies have been  
33 conducted in buffered, controlled environments within batch experiments, which may not accurately reflect  
34 manganese oxide behavior in more complex, heterogeneous soil (Chien et al., 2009; Fukuzumi et al., 1975; Liao et  
35 al., 2021; Liu et al., 2011; McBride, 1987; McKenzie, 1971; Shindo and Huang, 1984; Stone and H, 1989; Trainer et  
36 al., 2021). To the best of our knowledge, only a few works have investigated the oxidation of phenolic pollutants by  
37 manganese oxides in situ in soils. For instance, studies have shown the oxidation of phenolic acids and dissolved  
38 organic matter by manganese oxides in soils, but these works focused on naturally occurring, non-contaminating  
39 compounds rather than phenolic pollutant fate in the soil (Ding et al., 2022; Lehmann et al., 1987). In a study by  
40 Grebel et al. (Grebel et al., 2016), the oxidation of various phenolic contaminants was investigated using engineered  
41  $\text{MnO}_2$ -coated sand columns, and their key conclusion underscores  $\text{MnO}_2$  efficacy as an oxidizing agent for phenolic  
42 contaminants. However, to determine whether  $\text{MnO}_2$  can be equally effective in natural soil environments, further  
43 investigation is required.

44 We aim to investigate the fate of phenolic pollutants, specifically in the context of oxidation processes in  $\text{MnO}_2$ -  
45 enriched soil. To achieve this, we will apply both classical methodologies and an advanced geoelectrical method  
46 recently introduced to soil science: spectral induced polarization (SIP) (Gao et al., 2019; Johansson et al., 2019;  
47 Mellage et al., 2022; Revil, 2012; Schwartz et al., 2012; Schwartz and Furman, 2012; Shefer et al., 2013; Vaudelet et  
48 al., 2011; Vinegar and Waxman, 2012; Zhang et al., 2012). This approach allows us not only to track the  
49 transformation of phenolic pollutants through oxidation by  $\text{MnO}_2$  but also to monitor the broader impacts of this  
50 oxidation process on other elements within the soil environment.

51 SIP is a method where a low frequency, time dependent electrical field is applied, and the resultant potential is  
52 recorded. This technique captures both the conductive and capacitive characteristics of the subsurface, characterized  
53 by the in-phase ( $\sigma'$ ) and quadrature ( $\sigma''$ ) conductivity, respectively, in a non-invasive way (Binley and Kemna, 2005;  
54 Reynolds, 2011). Quadrature and in-phase conductivity are associated with the interfacial chemistry of the grain  
55 surface and grain size, while in-phase conductivity is also related to pore-water electrolyte conductivity (Ben Moshe  
56 and Furman, 2022). The  $\sigma''$  is frequency dependent and related to polarization processes at the electric double layer



57 (EDL), and indeed Vinegar & Waxman (Vinegar and Waxman, 2012) proposed a linear relationship between the soil  
58 cation exchange capacity (CEC) and the  $\sigma''$ . Additionally, studies on the impact of organic contaminants on the low-  
59 frequency complex conductivity of soils and porous materials demonstrated the ability of the SIP method to detect  
60 and monitor organic contaminants within the subsurface (Kirmizakis et al., 2020; Mellage et al., 2018, 2022; Revil,  
61 2012; Schwartz et al., 2020; Schwartz and Furman, 2012, 2015; Vaudelet et al., 2011).

62 This study aims to thoroughly explore the behavior of hydroquinone, a model phenolic molecule with a well-known  
63 oxidation mechanism by Mn-oxides, in MnO<sub>2</sub>-enriched sandy soil (Mn-sandy soil). To achieve this, we employed an  
64 array of methods including; electric measurements of the soil profile, crystallographic and microscopic examination  
65 of the soil minerals, and chemical analysis of the soil solution. We hypothesized that integrating electrical  
66 measurements, soil solution analysis, and soil surface examinations would enable us to reach a unique understanding  
67 of the oxidation process in the soil and provide insights into the resulting chemical mechanisms in the soil  
68 environment.

## 69 2. Materials and Methods

70 In this study, we investigated the oxidation of hydroquinone by MnO<sub>2</sub> in sandy soil column experiments. The  
71 experiments were conducted using sandy soil and MnO<sub>2</sub>-enriched sandy soil (Mn-sandy soil) to observe the behavior  
72 of hydroquinone and its oxidation product, benzoquinone. During the experiments, we employed SIP measurements  
73 to study the electrical characteristics of the soil as the oxidation process occurred. We analyzed the samples for  
74 hydroquinone and benzoquinone concentrations using High-Performance Liquid Chromatography (HPLC), and  
75 measured ion concentrations and composition by Coupled Plasma Atomic Emission Spectrometer (ICP-AES), pH,  
76 and Electrical Conductivity (EC). Additionally, we conducted Scanning Electron Microscopy (SEM), Energy-  
77 Dispersive X-ray Spectroscopy (EDS), and X-ray Diffraction (XRD) analyses to observe any changes in soil  
78 morphology and mineralogy before and after the introduction of hydroquinone to the soil.

### 79 2.1. Materials

80 Hydroquinone (99% purity), benzoquinone (99% purity), acetonitrile (HPLC grade), and calcium chloride were  
81 purchased from Sigma-Aldrich. Potassium permanganate, and hydrochloride acid 32% were purchased from Mercury  
82 LTD. Sandy soil with 97% sand and 3% silt (measured using PRIO, Meter group, Germany), contains 4% CaCO<sub>3</sub>, and  
83 2.5% organic matter.

### 84 2.2. MnO<sub>2</sub> preparation

85 MnO<sub>2</sub> was synthesized following the procedure of McKenzie (McKenzie, 1971). In brief, concentrated HCl was added  
86 dropwise to a boiling solution of potassium permanganate to form a dark purple precipitate of  $\delta$ -MnO<sub>2</sub>. After synthesis,  
87 the suspension was centrifuged (15,200 g, 15 min), and the supernatant was decanted and replaced with double-  
88 deionized water. The procedure was repeated until the supernatant was colorless; then the slurry was oven-dried  
89 overnight at 35 °C and freeze-dried.



90 **2.3. Methods**

91 **2.3.1. Spectral induced polarization measurements**

92 In the SIP method, a low frequency (typically 0.01 Hz to 10 kHz) oscillating current  $I$  (A) is applied through two  
93 electrodes on a porous medium, and electrical potential  $U$  (V) is measured by two other electrodes. Using Ohm's law,  
94 the complex admittance of the medium,  $Y^* = I/U$  (S) is obtained. The complex conductivity is related to the  
95 admittance through the geometric factor  $G$  ( $\text{m}^{-1}$ ) such that  $\sigma^* = G \cdot Y^*$ . The complex conductivity signal can be  
96 expressed as  $\sigma^* = \sigma' + i\sigma'' = |\sigma^*|e^{i\varphi}$ , where  $\sigma'$  ( $\text{S m}^{-1}$ ) is the in-phase conductivity, associated with energy  
97 dissipation processes,  $\sigma''$  ( $\text{S m}^{-1}$ ) is the quadrature conductivity, related to energy storage processes (Schwartz and  
98 Furman, 2012), and  $\varphi$  (rad) is the phase shift.

99 The SIP signal was measured using the PSIP impedance spectrometer (Ontash & Ermac Inc, NJ, USA), in polyvinyl  
100 chloride (3 cm diameter, 30 cm long) columns equipped with 4 brass electrodes, 6 mm in diameter, for both current  
101 injection and potential measurement (Fig.1). The current electrodes were 8 cm long and they crossed the entire sample,  
102 while the potential electrodes were 5 cm long, and they were retraced in their respective holes to prevent electrode  
103 polarization (as suggested by Cassiani et.al (Cassiani et al., 2009), and Schwartz and Furman (Schwartz and Furman,  
104 2012). Electrical contact between the potential electrodes and the sample was ensured through the electrolyte. The  
105 geometric factor ( $G$ ) was determined by measuring the admittance of a series of electrolytes with different electrical  
106 conductivities.

107

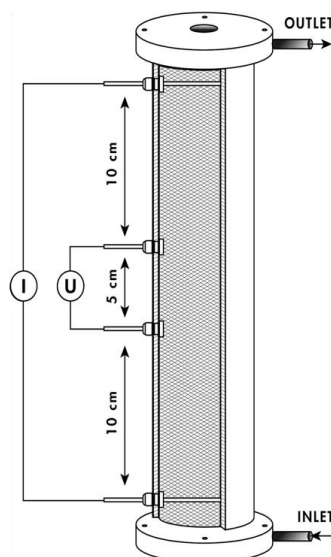


Figure 1. Scheme of experimental SIP column: inlet solution is injected in through the bottom and the outlet is collected in fractions. The current ( $I$ ) is injected between the top and the bottom electrodes, and the SIP signal is measured between the potential electrodes ( $U$ )



### 108 2.3.2. Column experiments

109 Breakthrough experiments were conducted to study the behavior of hydroquinone, and benzoquinone in sandy soil  
110 and Mn-sandy soil in an unbuffered environment. Two sets of experiments were performed using triplicate columns  
111 for each treatment: untreated sandy soil and Mn-sandy soil, which was prepared by mixing sandy soil with 5% w/w  
112 MnO<sub>2</sub>. Air-dried soil was mixed with 10% w/w of CaCl<sub>2</sub> 5mM solution as the saturating liquid. This soil was then  
113 packed in the columns in approximately 100 mL increments and gently compressed after each addition. Based on an  
114 assumed particle density of 2.65 g cm<sup>-3</sup> (Warrick, 2002), the average porosity of the sandy soil and Mn-sandy soil  
115 samples was 0.4 and 0.44±0.02, respectively.

116 After packing, the columns were placed vertically and a 5mM CaCl<sub>2</sub> solution was introduced from the bottom to wash  
117 away excess salt, ensuring saturated flow at a constant flow rate of 1 mL/min using a peristaltic pump (Masterflex L/S  
118 series, Cole-Parmer Inc., IL, USA). The soil was washed with CaCl<sub>2</sub> until equilibrium was reached between the inlet  
119 and outlet solutions (EC=900 μS cm<sup>-1</sup>). Upon reaching equilibrium, the inlet solution was replaced by a mixed solution  
120 of hydroquinone and benzoquinone (0.1M each in CaCl<sub>2</sub> 5mM solution), or by a hydroquinone solution (0.1M in  
121 CaCl<sub>2</sub> 5mM solution) passing through the sandy soil and Mn-sandy soil columns for 4 or 8 pore volumes (PV),  
122 respectively, until mass balance was achieved. Both solutions were left unbuffered and unpurged to better represent  
123 natural conditions.

124 Throughout the experiments, continuous SIP measurements were taken, and at 20-minute intervals, 2 mL samples of  
125 the outlet solution were collected and immediately filtered using a 0.22 μm reverse cellulose membrane filter syringe  
126 for further analysis. The collected outflow was analyzed to determine (1) hydroquinone and benzoquinone  
127 concentrations using HPLC (Waters 600, Waters, Milford, MA), equipped with a diode-array detector. The HPLC  
128 column was an XBridge Phenyl 3.5 μm 4.6X150 mm, with a flow rate of 1 mL/min, and the column temperature was  
129 set to 25 °C. Hydroquinone and benzoquinone were monitored at wavelengths of 222 nm and 246 nm, respectively.  
130 The mobile phase consisted of acetonitrile and double distilled water (DDW). The phase gradient started at 5%  
131 acetonitrile for 0-3 min, linearly increased to 40% for 3-10 min, and then increased again to 95% over 10-11 min.  
132 Acetonitrile maintained at 95% over 11-12 min, then decreased back to 5% over 12-13 min, and maintained at 5% for  
133 13-16 min. (2) Ca<sup>2+</sup> and soluble Mn concentration in the effluent by ICP-AES (Arcos Spectro Ltd., Germany), and  
134 (3) pH and EC values.

### 135 2.3.3. Colloid surface analysis by SEM-EDS and XRD

136 Sandy soil, MnO<sub>2</sub>, and Mn-sandy soil morphology was observed, before and after the introduction of hydroquinone  
137 by SEM (JEOL IT 100 Low vacuum). All samples were oven-dried at 40°C and thinly ground before analysis,  
138 mounted on 30 mm round SEM aluminum stubs using adhesive carbon tape. Secondary electron images were taken  
139 using the following operating conditions: 20 keV, 9 mm WD, and x350 magnification for all samples. For each soil,  
140 10 images were obtained and scanned for calcium, manganese, and silica semi-quantitative percentages, using EDS.  
141 The concentration of the elements in the Mn-sandy soil samples was corrected to the relative addition of Mn to the  
142 system. The effect of hydroquinone oxidation on Ca and Mn content in the soil was conducted using a non-parametric



143 comparison for each pair, using the Wilcoxon method. The statistical analysis was carried out by JMP®, Version 16.  
144 SAS Institute Inc.

145 The mineralogy of the soil and the change in MnO<sub>2</sub> mineralogy, pre- and post-oxidation were also evaluated by XRD.  
146 Soil samples were ground and loaded into an XRD sample holder by front loading followed by razor blade leveling.  
147 XRD patterns were acquired in Bragg-Brentano geometry using a PANalytical X'Pert diffractometer with CuK $\alpha$   
148 radiation operated at 45 kV and 40 mA. The samples were scanned from 5 to 70° 2 $\theta$  at a step size of 0.013° 2 $\theta$ , using  
149 a PIXcel detector in continuous scanning line (1D) mode with an active length of 3.35°. Mineral phase identification  
150 was performed using HighScore Plus® software based on the ICSD database.

### 151 3. Results and Discussion

#### 152 3.1. Hydroquinone and benzoquinone fate in sandy soils - breakthrough curves

153 Figure 2 illustrates the breakthrough curves of hydroquinone and benzoquinone in sandy soil (Fig. 2a) and Mn-sandy  
154 soil (Fig. 2b) columns. In the control sandy soil columns (Fig. 2a), both hydroquinone and benzoquinone exhibited  
155 classic symmetric sigmoidal breakthrough curves, with the breakthrough occurring at approximately 1 pore volume  
156 (PV). This suggests that there was negligible adsorption or chemical transformation of these compounds in the sandy  
157 soil, allowing them to pass through the column relatively unimpeded. In contrast, the breakthrough curves in the Mn-  
158 sandy soil columns (Fig. 2b) demonstrate different behavior. Benzoquinone showed an initial breakthrough at around  
159 4 PVs, reaching a relative concentration ( $C/C_0$ ) of about 0.2, and continued to increase gradually. Hydroquinone,  
160 however, exhibited a significantly delayed breakthrough, occurring at approximately 7 PVs with a relative  
161 concentration of 0.7. The moderate slopes of these breakthrough curves compared to the steep slopes observed in the  
162 sandy soil columns indicate that hydroquinone undergoes oxidation in the presence of MnO<sub>2</sub>, forming benzoquinone.  
163 This oxidation process is responsible for the delayed and more gradual breakthrough of hydroquinone, highlighting  
164 the reactive nature of the Mn-sandy soil in altering the transport and fate of these pollutants (Buamah et al., 2009).  
165

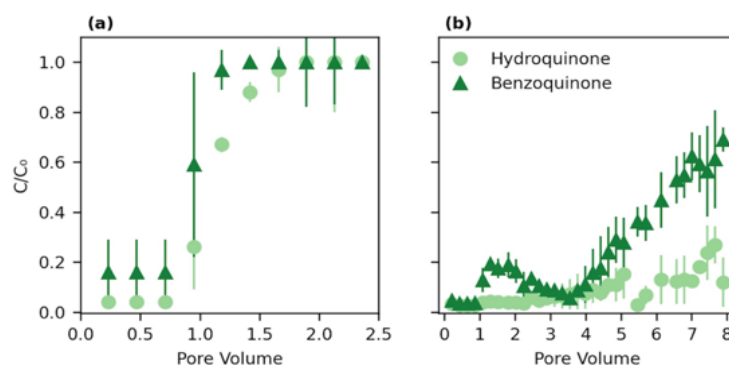


Figure 2. Hydroquinone (0.1 M initial) and benzoquinone (0.1M) relative concentrations, in (a) sandy soil and (b) Mn-sandy soil columns



167 **3.2. SIP and soil solution chemistry monitoring**

168 Sandy soil (control) and Mn-sandy soil columns were saturated with a background solution (5 mM CaCl<sub>2</sub>) and their  
 169 SIP signatures were recorded upon reaching equilibrium, before the introduction of the pollutant (Fig. 3).

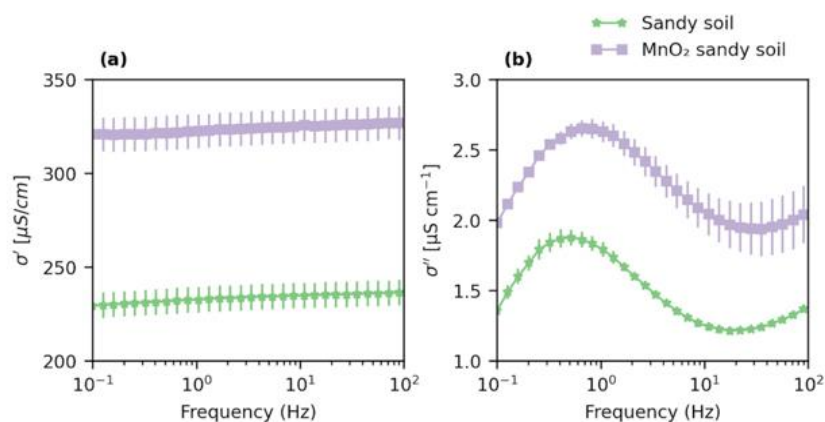


Figure 3. In-phase ( $\sigma'$ ) (a) and quadrature ( $\sigma''$ ) (b) conductivity of sandy and Mn-sandy soils (5 % w/w).

170

171 The quadrature conductivity ( $\sigma''$ ) (associated with surface polarization) of the sandy soil, exhibited classical spectra  
 172 for frequency-dependent polarization of porous media, with a peak at around 0.5 Hz (Fig. 3**Error! Reference source**  
 173 **not found**.b). Compared to the sandy soil,  $\sigma''$  of Mn- sandy soil increased by  $\sim 40\%$ , most likely due to the  
 174 contribution of the high CEC of MnO<sub>2</sub> (Händel et al., 2013; McKenzie, 1971; Post, 1999). Similarly, the in-phase  
 175 conductivity  $\sigma'$  was also higher ( $\sim 40\%$ ) than that of the sandy soil (Fig. 3a), most probably due to the contribution  
 176 of MnO<sub>2</sub> to the surface conductivity of the media (recall, that the EC of the soil solution was kept constant between  
 177 the treatments). Upon the addition of hydroquinone, the control columns demonstrated no change in both  $\sigma''$  and  $\sigma'$   
 178 throughout the experiment (Fig. 4a, b). This was accompanied by negligible benzoquinone, Ca<sup>2+</sup> and manganese  
 179 concentrations measured in the effluent. Additionally, the EC remained constant at  $1 \text{ mS m}^{-1} \pm 0.3$  and the pH values  
 180 were steady at  $9 \pm 0.2$  (Fig 5. a, b). These results indicate that there was neither adsorption nor oxidation of  
 181 hydroquinone in the control columns, as also demonstrated by the breakthrough curves (Figure 2a).

182 Hydroquinone flows through Mn-sandy soil columns induced a constant decrease in  $\sigma''$ , as expected, due to oxidation  
 183 processes in the system, resulting in a reduction in oxidizing and polarizing surfaces (Fig. 4 c, e). On the other hand,  
 184 the  $\sigma'$  increased up to  $\sim 4$  PVs and then decreased (Fig. 4 d, f). The maximum  $\sigma'$  value reached post  $\sim 4$  PVs  
 185 corresponded with peaks in EC and pH values, as well as Ca<sup>2+</sup> concentration in the effluents (Fig 5. c, d). The pH  
 186 value and EC dramatically increased from  $8.82 (\pm 0.25)$  and  $1.7 \text{ mS m}^{-1} (\pm 0.4)$  to  $10.8 (\pm 0.1)$  and  $4.53 \text{ mS m}^{-1} (\pm 0.03)$ ,  
 187 respectively (Fig. 5 c). Simultaneously, the Ca<sup>2+</sup> concentrations increased noticeably (from 0.1 to 25 mM) while the  
 188 manganese concentrations increased only slightly (from below the detection limit to 0.1 mM) (Fig 5. d). Indeed,  $\sigma'$  is  
 189 related to the bulk solution properties, i.e., an increase in ion concentration, mainly Ca<sup>2+</sup>, will result in an increase in





190  $\sigma'$ . Notably, all maxima for  $\text{Ca}^{2+}$ , EC,  $\sigma'$ , and pH corresponded with hydroquinone oxidation, as shown by  
191 benzoquinone breakthrough (Fig. 2b). Since these trends are not observed in the control sandy soil columns (with  
192 hydroquinone flow, but without  $\text{MnO}_2$ ) we suggest that hydroquinone oxidation by  $\text{MnO}_2$  surfaces initiated a cascade  
193 of reactions: (i) a local increase in proton concentration due to hydroquinone deprotonation decreasing the local pH  
194 (Rudolph et al., 2013). At this stage two reactions, which require protons, may take place simultaneously but at  
195 different rates: (iia) calcite dissolution (evident by the  $\text{Ca}^{2+}$ , EC,  $\sigma'$ , and pH measurements), and (iib)  $\text{MnO}_2$  reduction  
196 and dissolution to  $\text{Mn}^{2+/3+}$  (Fukuzumi et al., 1975; McBride, 1987; Remucal and Ginder-Vogel, 2014; Stone and H,  
197 1989), evident by benzoquinone breakthrough. The kinetics of calcite acid dissolution is at least 8 orders of magnitude  
198 higher than oxide acid dissolution (Anon, 2004) i.e., the protons are consumed faster by the calcite than by the  
199 oxidation reaction. (iii) The oxidation processes diminish, due to adsorption or precipitation of  $\text{Mn}^{2+/3+}$  as amorphous  
200 Mn-oxides on the birnessite ( $\text{MnO}_2$ ) surface (Ding et al., 2022; Remucal and Ginder-Vogel, 2014; Stone and H, 1989),  
201 also supported by the very low manganese concentrations eluting (0.1 mM). (iv) Calcite dissolution is suppressed,  
202 resulting in a decrease in  $\text{Ca}^{2+}$ , EC,  $\sigma'$ , and pH. Indeed, the decrease in  $\sigma''$  reflects the reduction in  $\text{CaCO}_3$  content in  
203 the soil (Izumoto et al., 2020; Wu et al., 2010) and may also correlate to a reduction in active  $\text{MnO}_2$  surfaces. To  
204 further support this suggested cascade of reactions, we tested the precipitation of  $\text{Mn}^{+2/+3}$  as amorphous Mn-oxides.



205

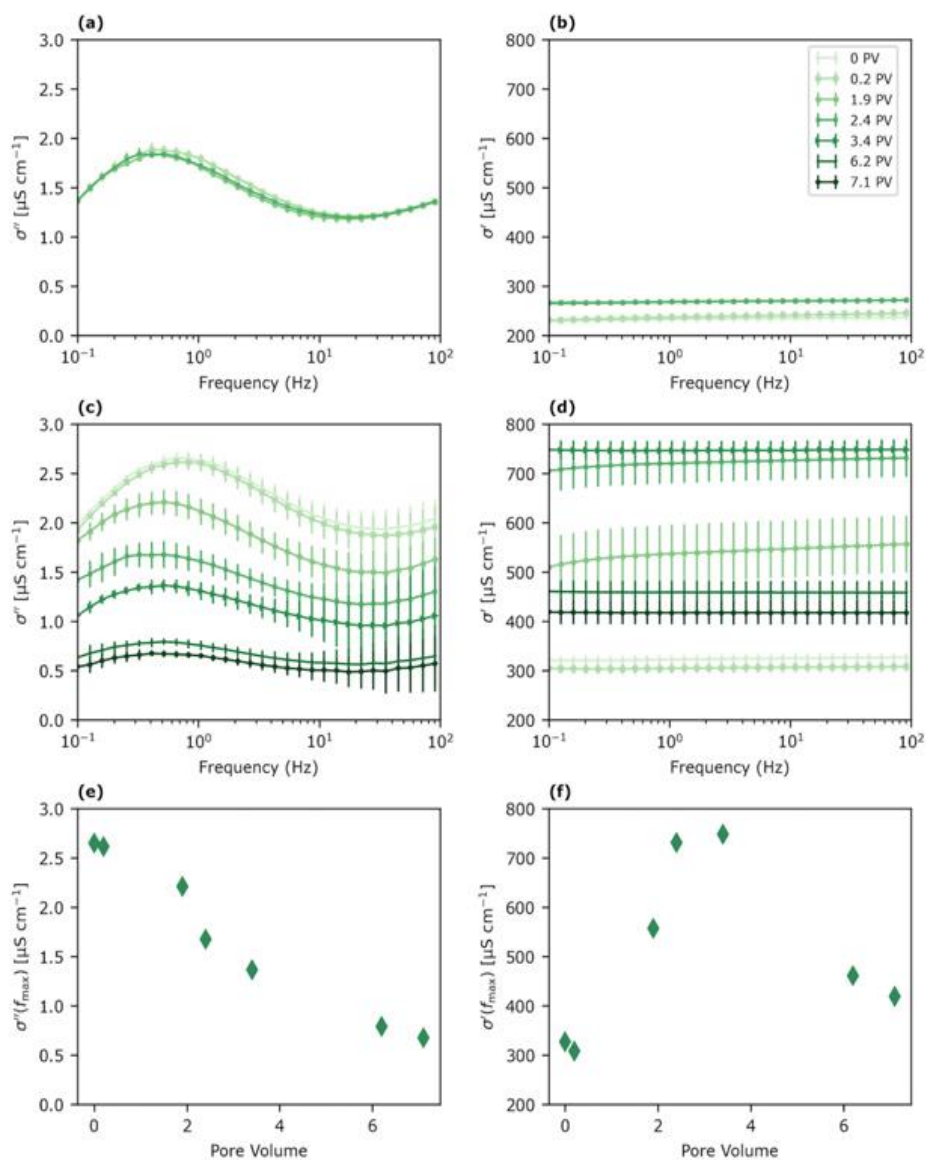


Figure 4. Quadrature ( $\sigma''$ ) and in-phase ( $\sigma'$ ) conductivity of sandy (a,b) and Mn-sandy soils (c,d) during hydroquinone oxidation.  $\sigma''$  (e) and  $\sigma'$  (f) at the peak frequency of Mn-sandy soil

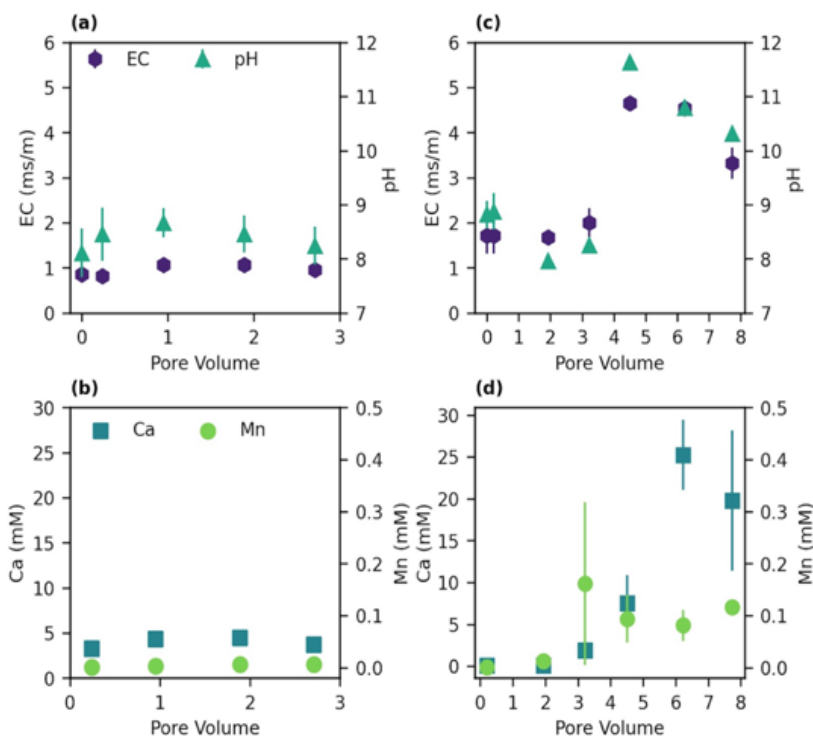


Figure 5. Effluent measurements of EC, pH, Ca<sup>2+</sup> and Mn concentrations in (a), (b) sandy and (c), (d) Mn-sandy soil

### 206 3.3. Soil mineral characterization

207 To further test MnO<sub>2</sub> dissolution and Mn<sup>2+/3+</sup> precipitation, we characterized the soil samples before and after  
 208 hydroquinone oxidation using XRD (Fig. 6a). The sandy soil was found to be composed mainly of quartz, feldspar,  
 209 and calcite. X-ray diffractogram analysis confirmed that the Mn-sandy soil initially contained approximately 5% of  
 210 MnO<sub>2</sub>. After hydroquinone oxidation, the MnO<sub>2</sub> content was reduced to ~ 1%, indicating that Mn<sup>4+</sup> was most likely  
 211 reduced to Mn<sup>2+/3+</sup>. These reduced manganese ions likely precipitated as amorphous Mn-oxides or were adsorbed  
 212 onto the MnO<sub>2</sub> surface, which would not be detected by XRD. This conclusion is further supported by the very low  
 213 concentration of Mn<sup>2+/3+</sup> eluting from the columns (Fig. 5b, d).

214 Finally, SEM images coupled with EDS analysis of the samples (2 replicates, 10 images per sample) confirm the  
 215 reduction in Ca content post oxidation, while the Mn content remains constant in both samples (Fig. 6 b). SEM images  
 216 vividly depict the morphology of pure MnO<sub>2</sub> (Fig. 6c), quartz, and CaCO<sub>3</sub> deposits in the sandy soil samples (Fig.  
 217 6d). In the Mn-sandy soil samples, MnO<sub>2</sub> is also notably present (Fig. 6e). Comparisons of post-oxidation samples to  
 218 pre-oxidation samples showed no significant visual changes (Fig 6. e, f).

219  
 220



221

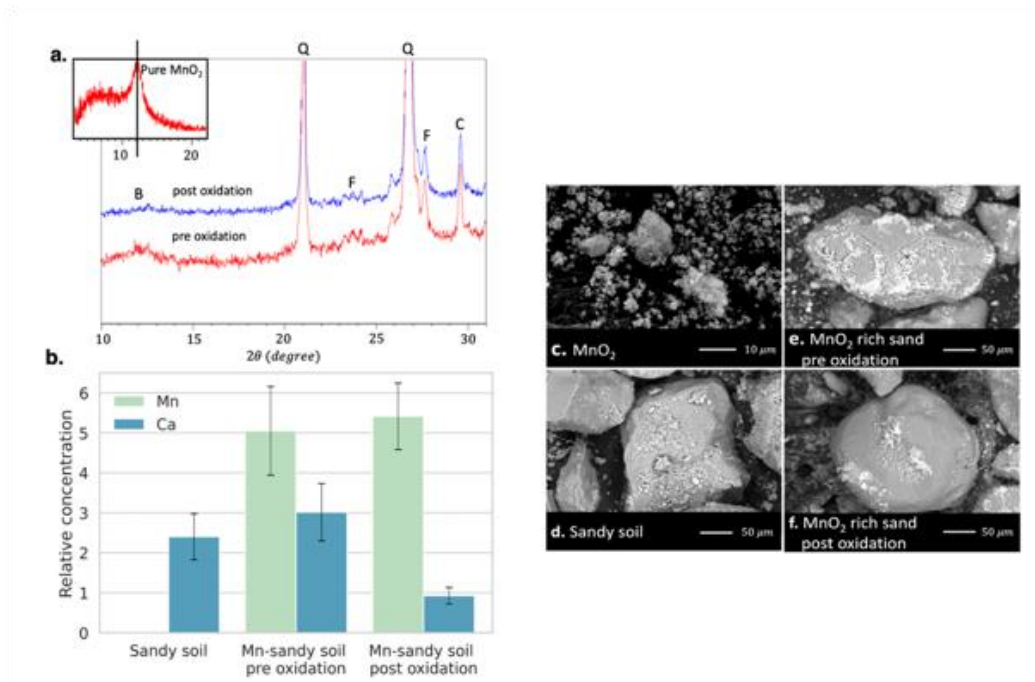


Figure 6. (a) X-ray diffraction full characterization curve of Mn-sandy soil, pre and post oxidation, and  $MnO_2$  inset. B, Q, F, and C represents the peaks of birnessite, quartz, feldspar, and calcite (b) Ca and Mn relative concentration by EDS analysis, and scanning electron micrographs of (c)  $MnO_2$ , (d) sandy soil, (e)  $MnO_2$  rich sandy soil, and (f)  $MnO_2$  rich sandy soil post oxidation.

#### 222 4. Conclusion

223 We explored the oxidation mechanism of hydroquinone in Mn-sandy soil by applying a combination of methods,  
 224 including electrical measurements (SIP), crystallographic analysis (XRD), microscopic examination (SEM-EDS) of  
 225 soil minerals, and chemical assessments of the soil solution (HPLC, ICP, pH, EC, etc.). Integrating results from these  
 226 different methods provided insights into subsequent reactions such as mineral dissolution, chemical precipitation, and  
 227 leaching.

228 Our findings suggest that hydroquinone oxidation by  $MnO_2$  surfaces to benzoquinone initiated a cascade of reactions  
 229 starting with local alterations in pH levels. These triggers increased  $CaCO_3$  dissolution, while simultaneously,  $MnO_2$   
 230 reduction results in its dissolution to  $Mn^{2+/3+}$  and adsorption or precipitation as amorphous Mn-oxides on the  $MnO_2$   
 231 surface. These results were supported by both chemical and electrical measurements.  $CaCO_3$  dissolution was identified  
 232 by a reduction in Ca by SEM-EDS analysis and by the SIP signature, showing a consistent decline in  $\sigma''$  due to a  
 233 reduction in polarized surfaces. The changes in  $Ca^{2+}$  concentrations in the effluent were monitored by ICP and  
 234 reflected by the alternating  $\sigma'$  signature. The effluent contained only minimal Mn concentration. XRD and SEM-EDS  
 235 analysis results demonstrated a reduction in  $MnO_2$  content and constant Mn content, respectively.



236 These combined findings support the precipitation of  $Mn^{2+3+}$  as amorphous Mn-oxides and  $MnO_2$  surface passivation,  
237 most likely also contributing to the consistent decrease in  $\sigma''$ . This study has provided valuable insights into the  
238 sensitivity of SIP signatures to changes in soil properties, due to oxidation processes within the soil. Future research  
239 should include the dynamic role of microbial activity in altering soil redox conditions, leading to  $MnO_2$  reduction or  
240  $CaCO_3$  dissolution. Furthermore, deeper exploration into the implications of soil structure changes resulting from  
241  $CaCO_3$  dissolution and precipitation on the fate of pollutants in the subsurface is necessary, considering diverse  
242 pollutant groups, organic matter, etc. In natural environments and at field scale, the complexities will require further  
243 investigation, potentially formulating effective environmental remediation strategies.

244

#### 245 **Competing interests**

246 The contact author has declared that none of the authors has any competing interests

#### 247 **Acknowledgments**

248 This research was supported by grant 80689 from the Ministry of Innovation, Science and Technology of Israel. We  
249 also acknowledge The Hebrew University of Jerusalem for internal funding.

#### 250 **References**

- 251 Ahmed, A. A., Thiele-Bruhn, S., Aziz, S. G., Hilal, R. H., Elroby, S. A., Al-Youbi, A. O., Leinweber, P., and Kühn,  
252 O.: Interaction of polar and nonpolar organic pollutants with soil organic matter: Sorption experiments and molecular  
253 dynamics simulation, *Sci. Total Environ.*, 508, 276–287, <https://doi.org/10.1016/J.SCITOTENV.2014.11.087>, 2015.
- 254 Anon: A COMPILATION OF RATE PARAMETERS OF WATER-MINERAL INTERACTION KINETICS FOR  
255 APPLICATION TO GEOCHEMICAL MODELING, 2004.
- 256 Ben Moshe, S. and Furman, A.: Real-time monitoring of organic contaminant adsorption in activated carbon filters  
257 using spectral induced polarization, *Water Res.*, 212, 118103, <https://doi.org/10.1016/j.watres.2022.118103>, 2022.
- 258 Binley, A. and Kemna, A.: DC Resistivity and Induced Polarization Methods, *Hydrogeophysics*, 129–156,  
259 [https://doi.org/10.1007/1-4020-3102-5\\_5](https://doi.org/10.1007/1-4020-3102-5_5), 2005.
- 260 Buamah, R., Petrushevski, B., and Schippers, J. C.: Oxidation of adsorbed ferrous iron: kinetics and influence of process  
261 conditions, *Water Sci. Technol.*, 60, 2353–2363, <https://doi.org/10.2166/wst.2009.597>, 2009.
- 262 Bünemann, E. K., Bongiorno, G., Bai, Z., Creamer, R. E., Deyn, G. D., Goede, R. de, Fleskens, L., Geissen, V.,  
263 Kuypers, T. W., Mäder, P., Pulleman, M., Sukkel, W., Groenigen, J. W. van, and Brussaard, L.: Soil quality – A critical  
264 review, *Soil Biol. Biochem.*, 120, 105–125, <https://doi.org/10.1016/J.SOILBIO.2018.01.030>, 2018.
- 265 Cassiani, G., Kemna, A., Villa, A., and Zimmermann, E.: Spectral induced polarization for the characterization of  
266 free-phase hydrocarbon contamination of sediments with low clay content, *Surf. Geophys.*, 7, 547–562,  
267 <https://doi.org/10.3997/1873-0604.2009028>, 2009.
- 268 Chien, S. W. C., Chen, H. L., Wang, M. C., and Seshaiiah, K.: Oxidative degradation and associated mineralization of  
269 catechol, hydroquinone and resorcinol catalyzed by birnessite, *Chemosphere*, 74, 1125–1133,  
270 <https://doi.org/10.1016/j.chemosphere.2008.10.007>, 2009.



- 271 Davi, M. L. and Gnudi, F.: Phenolic compounds in surface water, *Water Res.*, 33, 3213–3219,  
272 [https://doi.org/10.1016/S0043-1354\(99\)00027-5](https://doi.org/10.1016/S0043-1354(99)00027-5), 1999.
- 273 Delgado-Moreno, L., Bazhari, S., Gasco, G., Méndez, A., Azzouzi, M. E., and Romero, E.: New insights into the  
274 efficient removal of emerging contaminants by biochars and hydrochars derived from olive oil wastes, *Sci. Total*  
275 *Environ.*, 752, 141838, <https://doi.org/10.1016/J.SCITOTENV.2020.141838>, 2021.
- 276 Ding, Z., Ding, Y., Liu, F., Yang, J., Li, R., Dang, Z., and Shi, Z.: Coupled Sorption and Oxidation of Soil Dissolved  
277 Organic Matter on Manganese Oxides: Nano/Sub-nanoscale Distribution and Molecular Transformation, *Environ.*  
278 *Sci. Technol.*, 56, 2783–2793, <https://doi.org/10.1021/acs.est.1c07520>, 2022.
- 279 Farhan Hanafi, M. and Sapawe, N.: A review on the water problem associate with organic pollutants derived from  
280 phenol, methyl orange, and remazol brilliant blue dyes, *Mater. Today Proc.*, 31, A141–A150,  
281 <https://doi.org/10.1016/j.matpr.2021.01.258>, 2020.
- 282 Fukuzumi, S.-I., Ono, Y., and Keii, T.: ESR Studies on the Formation of p-Benzosemiquinone Anions over Manganese  
283 Dioxide, *INTERNATIONAL JOURNAL OF CHEMICAL KINETICS*, 1975.
- 284 Gao, Z., Haegel, F.-H., Esser, O., Zimmermann, E., Vereecken, H., and Huisman, J. a.: Spectral Induced Polarization  
285 of Biochar in Variably Saturated Soil, *Vadose Zone J.*, 18, 180213, <https://doi.org/10.2136/vzj2018.12.0213>, 2019.
- 286 Grebel, J. E., Charbonnet, J. A., and Sedlak, D. L.: Oxidation of organic contaminants by manganese oxide geomedia  
287 for passive urban stormwater treatment systems, *Water Res.*, 88, 481–491,  
288 <https://doi.org/10.1016/j.watres.2015.10.019>, 2016.
- 289 Gusain, R., Gupta, K., Joshi, P., and Khatri, O. P.: Adsorptive removal and photocatalytic degradation of organic  
290 pollutants using metal oxides and their composites: A comprehensive review, *Adv. Colloid Interface Sci.*, 272,  
291 102009, <https://doi.org/10.1016/j.cis.2019.102009>, 2019.
- 292 Händel, M., Rennert, T., and Totsche, K. U.: A simple method to synthesize birnessite at ambient pressure and  
293 temperature, *Geoderma*, 193–194, 117–121, <https://doi.org/10.1016/j.geoderma.2012.09.002>, 2013.
- 294 Izumoto, S., Huisman, J. A., Wu, Y., and Vereecken, H.: Effect of solute concentration on the spectral induced  
295 polarization response of calcite precipitation, *Geophys. J. Int.*, 220, 1187–1196, <https://doi.org/10.1093/gji/ggz515>,  
296 2020.
- 297 Johansson, S., Rossi, M., Hall, S. A., Sparrenbom, C., Hagerberg, D., Tudisco, E., Rosqvist, H., and Dahlin, T.:  
298 Combining spectral induced polarization with X-ray tomography to investigate the importance of DNAPL geometry  
299 in sand samples, *Geophysics*, 84, E173–E188, <https://doi.org/10.1190/geo2018-0108.1>, 2019.
- 300 Jones, K. C., Alcock, R. E., Johnson, D. L., Semple, K. T., and Woolgar, P. J.: Organic chemicals in contaminated  
301 land : analysis, significance and research priorities., 1996.
- 302 Kang, S. H. and Choi, W.: Oxidative Degradation of Organic Compounds Using Zero-Valent Iron in the Presence of  
303 Natural Organic Matter Serving as an Electron Shuttle, *Environ. Sci. Technol.*, 43, 878–883,  
304 <https://doi.org/10.1021/ES801705F>, 2008.
- 305 Kirmizakis, P., Kalderis, D., Ntarlagiannis, D., and Soupios, P.: Preliminary assessment on the application of biochar  
306 and spectral-induced polarization for wastewater treatment, *Surf. Geophys.*, 18, 109–122,  
307 <https://doi.org/10.1002/nsg.12076>, 2020.
- 308 Komprda, J., Komprdová, K., Sánka, M., Možný, M., and Nizzetto, L.: Influence of climate and land use change on  
309 spatially resolved volatilization of persistent organic pollutants (POPs) from background soils, *Environ. Sci. Technol.*,  
310 47, 7052–7059, [https://doi.org/10.1021/ES3048784/SUPPL\\_FILE/ES3048784\\_SI\\_001.PDF](https://doi.org/10.1021/ES3048784/SUPPL_FILE/ES3048784_SI_001.PDF), 2013.



- 311 Lambert, J. F.: Organic pollutant adsorption on clay minerals, *Dev. Clay Sci.*, 9, 195–253,  
312 <https://doi.org/10.1016/B978-0-08-102432-4.00007-X>, 2018.
- 313 Lehmann, R. G., Cheng, H. H., and Harsh, J. B.: Oxidation of Phenolic Acids by Soil Iron and Manganese Oxides,  
314 *Soil Sci. Soc. Am. J.*, 51, 352–356, <https://doi.org/10.2136/sssaj1987.03615995005100020017x>, 1987.
- 315 Liao, X., Zhang, C., Nan, C., Lv, Y., Fan, Z., and Hu, L.: Phenol driven changes onto MnO<sub>2</sub> surface for efficient  
316 removal of methyl parathion: The role of adsorption, *Chemosphere*, 269, 128695,  
317 <https://doi.org/10.1016/j.chemosphere.2020.128695>, 2021.
- 318 Liu, M. M., Cao, X. H., Tan, W. F., Feng, X. H., Qiu, G. H., Chen, X. H., and Liu, F.: Structural controls on the  
319 catalytic polymerization of hydroquinone by birnessites, *Clays Clay Miner.*, 59, 525–537,  
320 <https://doi.org/10.1346/CCMN.2011.0590510>, 2011.
- 321 Loffredo, E. and Senesi, N.: Fate of anthropogenic organic pollutants in soils with emphasis on adsorption/desorption  
322 processes of endocrine disruptor compounds, *Pure Appl. Chem.*, 78, 947–961,  
323 <https://doi.org/10.1351/PAC200678050947/MACHINEREADABLECITATION/RIS>, 2006.
- 324 McBride, M. B.: Adsorption and Oxidation of Phenolic Compounds by Iron and Manganese Oxides, *Soil Sci. Soc.*  
325 *Am. J.*, 51, 1466–1472, <https://doi.org/10.2136/sssaj1987.03615995005100060012x>, 1987.
- 326 McKenzie, R. M.: The synthesis of birnessite, cryptomelane, and some other oxides and hydroxides of manganese,  
327 *Mineral. Mag.*, 38, 493–502, <https://doi.org/10.1180/MINMAG.1971.038.296.12>, 1971.
- 328 Mellage, A., Holmes, A. B., Linley, S., Vallée, L., Rezaezhad, F., Thomson, N., Gu, F., and Cappellen, P. V.: Sensing  
329 Coated Iron-Oxide Nanoparticles with Spectral Induced Polarization (SIP): Experiments in Natural Sand Packed  
330 Flow-Through Columns, *Environ. Sci. Technol.*, 52, 14256–14265,  
331 [https://doi.org/10.1021/ACS.EST.8B03686/SUPPL\\_FILE/ES8B03686\\_SI\\_001.PDF](https://doi.org/10.1021/ACS.EST.8B03686/SUPPL_FILE/ES8B03686_SI_001.PDF), 2018.
- 332 Mellage, A., Zakai, G., Efrati, B., Pagel, H., and Schwartz, N.: Paraquat sorption- and organic matter-induced  
333 modifications of soil spectral induced polarization (SIP) signals, *Geophys. J. Int.*, 229, 1422–1433,  
334 <https://doi.org/10.1093/GJI/GGAB531>, 2022.
- 335 Murray, J. W.: The surface chemistry of hydrous manganese dioxide, *J. Colloid Interface Sci.*, 46, 357–371,  
336 [https://doi.org/10.1016/0021-9797\(74\)90045-9](https://doi.org/10.1016/0021-9797(74)90045-9), 1974.
- 337 Post, J. E.: Manganese oxide minerals: Crystal structures and economic and environmental significance, *Proc. Natl.*  
338 *Acad. Sci. U. S. A.*, 96, 3447–3454, <https://doi.org/10.1073/PNAS.96.7.3447/ASSET/FCC9F2E4-0CCE-4282-9C0C-5C8274858495/ASSETS/GRAPHIC/PQ0694486002.JPEG>, 1999.
- 340 Reid, B. J., Jones, K. C., and Semple, K. T.: Bioavailability of persistent organic pollutants in soils and sediments—a  
341 perspective on mechanisms, consequences and assessment, *Environ. Pollut.*, 108, 103–112,  
342 [https://doi.org/10.1016/S0269-7491\(99\)00206-7](https://doi.org/10.1016/S0269-7491(99)00206-7), 2000.
- 343 Remucal, C. K. and Ginder-Vogel, M.: A critical review of the reactivity of manganese oxides with organic  
344 contaminants, *Environ. Sci. Process. Impacts*, 16, 1247–1266, <https://doi.org/10.1039/C3EM00703K>, 2014.
- 345 Revil, A.: Spectral induced polarization of shaly sands: Influence of the electrical double layer, *Water Resour. Res.*,  
346 48, <https://doi.org/10.1029/2011WR011260>, 2012.
- 347 Reynolds, J. M.: An Introduction to Applied and Environmental Geophysics, 712, 2011.
- 348 Rudolph, N., Voss, S., Moradi, A. B., Nagl, S., and Oswald, S. E.: Spatio-temporal mapping of local soil pH changes  
349 induced by roots of lupin and soft-rush, *Plant Soil*, 369, 669–680, <https://doi.org/10.1007/s11104-013-1775-0>, 2013.





- 350 Schwartz, N. and Furman, A.: Spectral induced polarization signature of soil contaminated by organic pollutant:  
351 Experiment and modeling, *J. Geophys. Res. Solid Earth*, 117, 10203, <https://doi.org/10.1029/2012JB009543>, 2012.
- 352 Schwartz, N. and Furman, A.: On the spectral induced polarization signature of soil organic matter, *Geophys. J. Int.*,  
353 200, 589–595, <https://doi.org/10.1093/GJI/GGU410>, 2015.
- 354 Schwartz, N., Huisman, J. A., and Furman, A.: The effect of NAPL on the electrical properties of unsaturated porous  
355 media, *Geophys. J. Int.*, 188, 1007–1011, <https://doi.org/10.1111/J.1365-246X.2011.05332.X/2/188-3-1007->  
356 FIG002.JPEG, 2012.
- 357 Schwartz, N., Levy, L., Carmeli, B., and Radian, A.: Spectral induced polarization of clay-oxide hybrid particles, *J.*  
358 *Colloid Interface Sci.*, 577, 173–180, <https://doi.org/10.1016/J.JCIS.2020.05.029>, 2020.
- 359 Shefer, I., Schwartz, N., and Furman, A.: The effect of free-phase NAPL on the spectral induced polarization signature  
360 of variably saturated soil, *Water Resour. Res.*, 49, 6229–6237, <https://doi.org/10.1002/WRCR.20502>, 2013.
- 361 Shindo, H. and Huang, P. M.: Catalytic Effects of Manganese (IV), Iron(III), Aluminum, and Silicon Oxides on the  
362 Formation of Phenolic Polymers, *Soil Sci. Soc. Am. J.*, 48, 927–934,  
363 <https://doi.org/10.2136/sssaj1984.03615995004800040045x>, 1984.
- 364 Stone, A. T. and H. H. U. L. R. I. C.: Kinetics and Reaction Stoichiometry in the Reductive Dissolution of  
365 Manganese(IV) Dioxide and Co(III) Oxide by Hydroquinone, 1989.
- 366 Sun, J., Mu, Q., Kimura, H., Murugadoss, V., He, M., Du, W., and Hou, C.: Oxidative degradation of phenols and  
367 substituted phenols in the water and atmosphere: a review, *Adv. Compos. Hybrid Mater.*, 5, 627–640,  
368 <https://doi.org/10.1007/s42114-022-00435-0>, 2022.
- 369 Trainer, E. L., Ginder-Vogel, M., and Remucal, C. K.: Selective Reactivity and Oxidation of Dissolved Organic Matter  
370 by Manganese Oxides, *Environ. Sci. Technol.*, 55, 12084–12094, <https://doi.org/10.1021/acs.est.1c03972>, 2021.
- 371 Vaudelet, P., Revil, A., Schmutz, M., Franceschi, M., and Bégassat, P.: Changes in induced polarization associated  
372 with the sorption of sodium, lead, and zinc on silica sands, *J. Colloid Interface Sci.*, 360, 739–752,  
373 <https://doi.org/10.1016/J.JCIS.2011.04.077>, 2011.
- 374 Vinegar, H. J. and Waxman, M. H.: Induced polarization of shaly sands, <https://doi.org/10.1190/1.1441755>, 49, 1267–  
375 1287, <https://doi.org/10.1190/1.1441755>, 2012.
- 376 Warrick, A. W. (Ed.): *Soil physics companion*, CRC Press, Boca Raton, FL, 389 pp., 2002.
- 377 Wu, Y., Hubbard, S., Williams, K. H., and Ajo-Franklin, J.: On the complex conductivity signatures of calcite  
378 precipitation, *J. Geophys. Res. Biogeosciences*, 115, <https://doi.org/10.1029/2009JG001129>, 2010.
- 379 Zhang, C., Slater, L., Redden, G. D., Fujita, Y., Johnson, T. J., Johnson, T. C., and Fox, D. T.: Spectral Induced  
380 Polarization Signatures of Hydroxide Adsorption and Mineral Precipitation in Porous Media, *Environ. Sci. Technol.*,  
381 46, 4357–4364, <https://doi.org/10.1021/es204404e>, 2012.
- 382